

Article

Functionalization of ZnO Nanorods with Au Nanodots via In Situ Reduction for High-Performance Detection of Ethyl Acetate

Qilin Wang ¹, Wei Wang ¹, Yizhuo Fan ¹, Jian Fang ¹, Yu Chen ^{2,*} and Shengping Ruan ^{1,*}

¹ College of Electronic Science & Engineering, Jilin University, Changchun 130012, China; wangql_icy@163.com (Q.W.); wangw_jlu@163.com (W.W.); fanyz97@163.com (Y.F.); fazeup@126.com (J.F.)

² Institute of Semiconductors, Chinese Academy of Sciences, Beijing 100083, China

* Correspondence: zhuq1226@aliyun.com (Y.C.); ruansp@jlu.edu.cn (S.R.); Tel.: +86-0431-85168242 (S.R.)

Abstract: Ethyl acetate is a critical medical indicator for detecting certain types of cancer. However, at present, available sensitive materials often exhibit drawbacks, such as high operating temperatures and poor responses to low concentrations of ethyl acetate. In this study, a ZnO nanorod sensing material was prepared using high-temperature annealing and a hydrothermally synthesized metal-organic framework (MOF) as a template. Au nanodots (AuNDs) were subsequently modified on the ZnO nanorods using an in situ ion reduction, which provided a better dispersion of Au nanodots compared with that obtained using the common reductant method. A variety of characterization methods indicate that the highly dispersed AuNDs, which possess a high catalytic activity, were loaded onto the surface as active centers, leading to a significant augmentation in the adsorption of oxygen on the surface compared with the original ZnO material. Consequently, the AuND@ZnO material exhibited heightened responsiveness to ethyl acetate at a lower operating temperature. The Au@ZnO-based sensor has a response rate (R_a/R_g) of 41.8 to 20 ppm ethyl acetate gas at 140 °C, marking a 17.4-fold increase compared with that of the original material. Due to its low power consumption and high responsiveness, AuND@ZnO is a promising candidate for the detection of ethyl acetate gas in medical applications.

Keywords: zinc oxide; nanorods; AuND functionalization; ethyl acetate; gas sensor



Citation: Wang, Q.; Wang, W.; Fan, Y.; Fang, J.; Chen, Y.; Ruan, S.

Functionalization of ZnO Nanorods with Au Nanodots via In Situ Reduction for High-Performance Detection of Ethyl Acetate. *Sensors* **2024**, *24*, 6931. <https://doi.org/10.3390/s24216931>

Academic Editor: Antonios Kelarakis

Received: 23 September 2024

Revised: 25 October 2024

Accepted: 26 October 2024

Published: 29 October 2024



Copyright: © 2024 by the authors. Licensee MDPI, Basel, Switzerland. This article is an open access article distributed under the terms and conditions of the Creative Commons Attribution (CC BY) license (<https://creativecommons.org/licenses/by/4.0/>).

1. Introduction

Ethyl acetate (EA), a common volatile organic compound pollutant, is a colorless and irritating gas with a low boiling point at atmospheric pressure. In the medical field, ethyl acetate can be detected in a patient's exhaled breath, so it can be used as clinical diagnostic evidence for colorectal cancer and stomach cancer [1,2]. Despite being generally considered less toxic, the harm it poses to the human body should not be underestimated. Ethyl acetate can irritate the ocular conjunctiva, nasal mucosa, and upper respiratory tract. Inhalation of ethyl acetate at a certain concentration can cause acute neurological anesthesia, pulmonary edema, leukocytosis, and in severe cases, kidney and liver damage [3]. Therefore, continuous monitoring of low concentrations of ethyl acetate in specific environments (such as hospitals and factories) holds significant importance [4]. These conditions necessitate sensors with low power consumption and high responsiveness to low concentrations of EA gas. Currently, high-precision detection of such volatile organic compounds can be achieved using RFID sensors, catalytic luminescence sensors, and electrochemical sensors, among others [5–7].

Metal-organic frameworks (MOFs) are porous crystal materials formed by the self-assembly of metal ions or metal clusters and organic ligands through coordination bonds. They possess adjustable pore structures, functional sites, and good hydrothermal stability [8–10]. Moreover, the derived oxides removed from the organic ligand bonds by annealing can inherit the morphology of the original MOF material. Among them, Zn-MOF-derived oxide materials exhibit

various crystal morphologies and a relatively large surface area, providing more surface reaction sites, which make them frequently employed in gas-sensing fields [11]. However, simple ZnO materials often demonstrate low gas-sensing properties, necessitating improvements through surface modification [12,13].

Noble metal nanodots have found wide applications in modifying catalytically sensitive materials owing to their excellent catalytic activity and electrical conductivity [14]. Gold nanodots (AuNDs), as the most significant member of the noble metal nanoparticle family, exhibit an electron spillover effect, significantly increasing the adsorbed oxygen ratio on the sensitive material's surface and facilitating the rapid transfer of electrons generated in surface gas reactions to the sensitive material [15]. The in situ reduction of Au nanodots by electrostatically adsorbed materials results in a smaller size than that of noble metal nanoparticles modified using common reduction methods. The resulting size effect will affect the ZnO lattice, which can further increase the proportion of adsorbed oxygen on the material surface [16]. The excellent chemical catalytic effect of AuNDs accelerates the surface reaction of some organic gas molecules, thereby significantly enhancing the response to specific gases and reducing the optimal operating temperature of the materials [17].

In this work, Zn-MOF nanorods were synthesized by coordinating zinc ions using homophenetic acid [H₃BTC] as the organic ligand. Ultrafine and highly dispersed gold nanodots were then synthesized on the nanorod surface via in situ reduction of HAuCl₄ [18]. Subsequent annealing yielded Au@ZnO nanorods that exhibit high gas sensitivity properties. Characterization using XPS, TEM, and other methods revealed that the modified AuNDs on ZnO nanorods effectively increased the adsorbed oxygen ratio on the material's surface, thereby enhancing the surface reaction rate for ethyl acetate gas. The good sensing characteristics of Au@ZnO sensors to target gas, including high responsiveness at low concentrations, low operating temperature, and admirable selectivity, can be attributed primarily to the unique electron spillover effect and good electrical conductivity of the surface AuNDs [19].

2. Experimental

2.1. Chemical Regent

Zn-MOF was synthesized using zinc nitrate hexahydrate (Zn(NO₃)₂·6H₂O) and 1,3,5-benzenetricarboxylic acid (H₃BTC), both purchased from Shanghai Aladdin Biochemical Technology Co., Ltd. (Shanghai, China). The chloroauric acid solution was prepared by dissolving chloroauric acid trihydrate (HAuCl₄·3H₂O) in deionized water according to a required ratio. All the solid reagents used were of analytical grade.

2.2. Materials Synthesis

The synthesis process is shown in Figure 1. First, Zn-MOF was prepared using a hydrothermal method [20]. Initially, 1.483 g of Zn(NO₃)₂·6H₂O and 1.6 g of H₃BTC were dissolved in 10 mL of ethanol, followed by the addition of 30 mL of DMF to the mixture. The solution was then stirred for 1 h before being transferred to a Teflon liner and heated at 85 °C for 20 h. After the hydrothermal reaction, the products were collected and cleaned three times with ethanol. Finally, the product was dried overnight in an oven at 70 °C. The resulting samples were Zn-MOF.

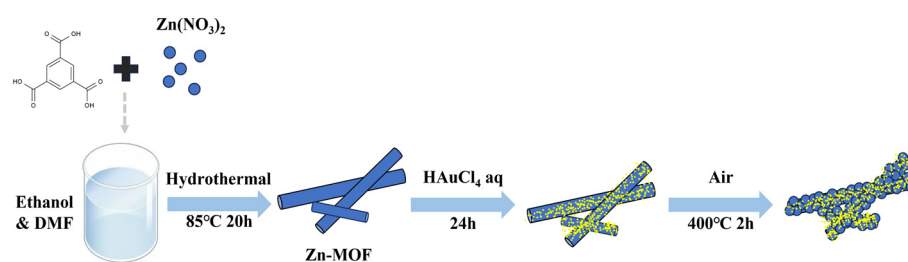


Figure 1. Schematic diagram of the synthesis process of AuND@ZnO nanorods.

Subsequently, Au nanodots were modified on the Zn-MOF using an in-situ reduction method. The Zn-MOF obtained was ultrasonically dispersed in deionized water, and varying amounts of HAuCl₄ solution, and a concentration of 20 mmol/L was added. The mixture was left for 24 h, after which the precipitate was collected. The final sample was obtained by annealing the Zn/Au-MOF in a muffle furnace at 400 °C for 2 h. The materials were named ZnAu-100, ZnAu-200, and ZnAu-400 according to the volume of HAuCl₄ solution added (100 µL, 200 µL, and 400 µL, respectively).

2.3. Fabrication and Measurement of Sensors

The preparation process of the gas sensor is as follows. First, the synthesized material is mixed with anhydrous ethanol at a mass ratio of 1:4 and ground into a suspension in an agate mortar. Then, the paste is uniformly applied to a ceramic substrate with an Au measuring electrode and a Ru heating electrode, and the sensor layer is formed after the anhydrous ethanol evaporates naturally. Finally, two sets of electrodes on the ceramic substrate are welded on a hexagonal seat accordingly. The sensor is aged for two days at the aging station. Gas sensitivity is assessed using a CGS-8 analytical system (Beijing Elite, Beijing, China) at a temperature of 20 °C and relative humidity of 25%. The dynamic gas distribution system DGL-3 equipped with a humidity module is employed to introduce the measured gas into the micro gas chamber of the CGS-8 analysis system. The resistance in air is denoted as R_a , while the resistance in the test gas is denoted as R_g . For N-type semiconductors, the sensor's response to reducing gases is calculated using the R_a/R_g ratio, whereas that to oxidizing gases is determined using the R_g/R_a ratio. Response/recovery time is defined as the time it takes for the resistance changed by 90% when the gas environment transitions.

2.4. Characterization

Crystal diffraction results were obtained using X-ray diffraction (XRD, Cu K α , 1.5418 µm; D/Max 2550, Rigaku, Japan). Sample morphology information was obtained using scanning electron microscopy (SEM; JSM-7500F, JEOL, Japan), and high-resolution lattice fringes were characterized using transmission electron microscopy (TEM; JEM-2100F, JEOL, Japan). The chemical states and surface compositions of the samples were analyzed using X-ray photoelectron spectroscopy (VG ESCALAB MK II, UN).

3. Results and Discussion

3.1. Material Characterizations

First, XRD characterization was performed to analyze the crystal structure. The XRD results of ZnO and ZnAu-200 samples are shown in Figure 2a. All patterns correspond to the characteristics of the ZnO phase (JCPDS No. 36-1451) and match the wurtzite crystal phase well. However, due to the low Au loadings, only the ZnO phase can be identified in the XRD pattern of ZnAu-200 [21].

The Tauc diagram in Figure 2b indicates that the band gaps (E_g) of ZnO and ZnAu-200 are 3.18 eV and 3.12 eV, respectively. A narrower E_g implies a smaller energy barrier for electron transfer, making it easier for electrons to be captured by oxygen molecules in air and form adsorbed oxygen, which is crucial for the detection of ethyl acetate gas. This contributes to enhanced gas-sensing performance [22].

XPS analysis confirmed that ZnAu-200 is composed of Zn, O, C, and Au elements. The Zn 3p region overlaps with the Au 4f region, as shown in Figure 3b. The double peaks at 88.3 eV and 91.2 eV belong to Zn 3p, and the double peaks at 86.4 eV and 89.5 eV belong to Au [23]. The binding energies of the Zn 2p region are 1045.3 eV and 1022.3 eV. Compared with the control group, the Zn 2p peak in the AuZn-200 group shifted by 0.8 eV toward the low binding energy, and the relative intensity decreased [23]. According to the literature, the Fermi level of Au is lower than that of ZnO [24]. Combined with XPS, the results show that electron transfer occurs between ZnO and AuNDs on the surface of the material, and a

Schottky junction is formed, which widens the material's internal electron depletion layer and increases the baseline resistance of the material [25].

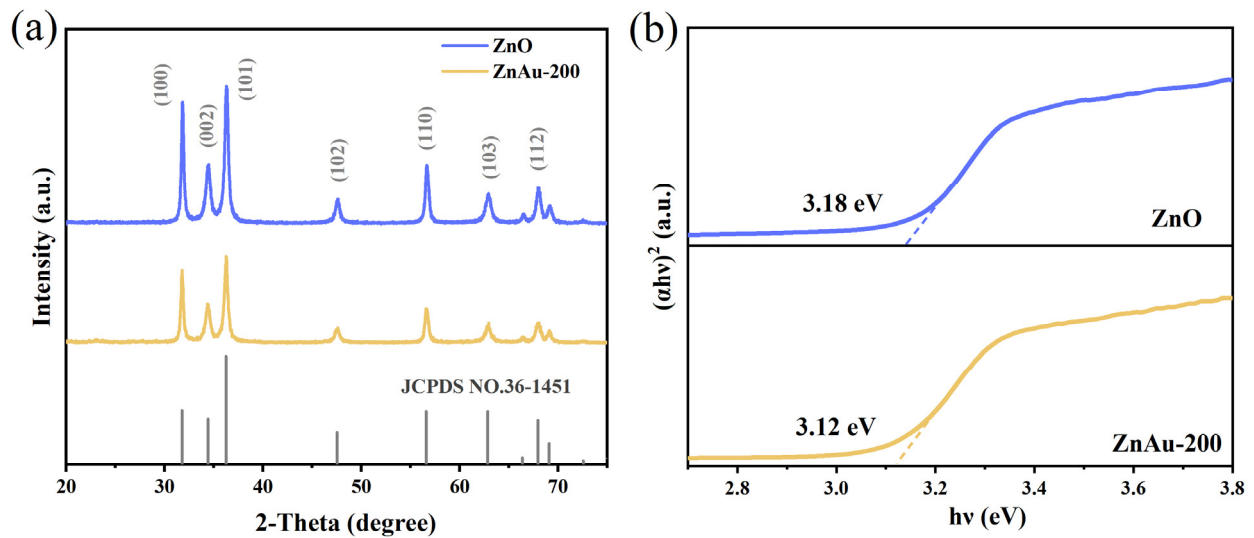


Figure 2. (a) XRD patterns of ZnAu-200 and pure ZnO materials; (b) Tauc diagram of ZnO and ZnAu-200.

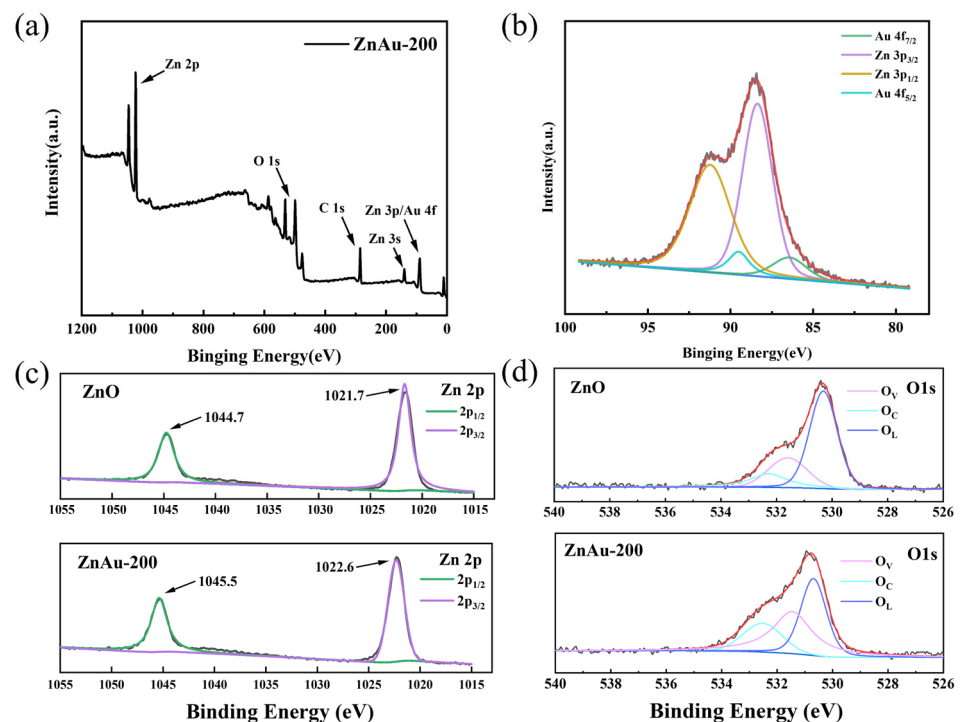


Figure 3. (a) Full XPS spectrum of ZnAu-200; (b) Zn 3p and Au 4f peaks resulting from the deconvolution operation; and (c) Zn 2p and (d) O 1s spectra of pure ZnO and ZnAu-200.

The gas-sensing property of the material is greatly affected by the proportion of oxygen adsorbed on the surface. Figure 3d shows the XPS spectrum of O 1s, which can be deconvoluted into three Gaussian peaks. The oxygen ion binding energy and relative proportions between the two materials are shown in Table 1. It can be concluded that the relative content of chemisorbed oxygen in the ZnAu-200 samples is greatly increased, which is conducive to more electron transfer on the surface of the material during the

surface reaction against the target gas [26]. Thus, the resistivity of the material has a great change, which is reflected in the increase in the response value.

Table 1. XPS spectra fitting results of oxygen species in ZnO and ZnAu-200.

Sample	Oxygen Species	Binding Energy (eV)	Relative Percentage (%)
ZnO	O _C (chemisorbed)	532.2	15.72%
	O _V (vacancy)	531.5	24.19%
	O _L (lattice)	530.3	60.08%
ZnAu-200	O _C (chemisorbed)	532.5	19.42%
	O _V (vacancy)	531.4	42.56%
	O _L (lattice)	530.6	38.00%

Figure 4 illustrates the microscopic morphology of the material under a scanning electron microscope. The precursor of the sample has a typical nanorod-like structure with length of about 100 nm, which is consistent with the morphology of the ZnO-MOF precursor material, indicating that the modification with Au nanodots does not change the original metal-organic framework morphology [27]. After the organic matter is removed by calcination, the AuND@ZnO material generally inherits the stick-like morphology of the precursor material, as shown in Figure 4c. Moreover, the multi-granular changes on the surface during calcination could increase the specific surface area of the material, exposing more of the active sites of the Au dots and enhancing contact areas with the gas molecules to be measured. Moreover, the nanorod morphology enables the axial transfer of electrons, which is more conducive to the sensing reaction on the surface of the material [28].

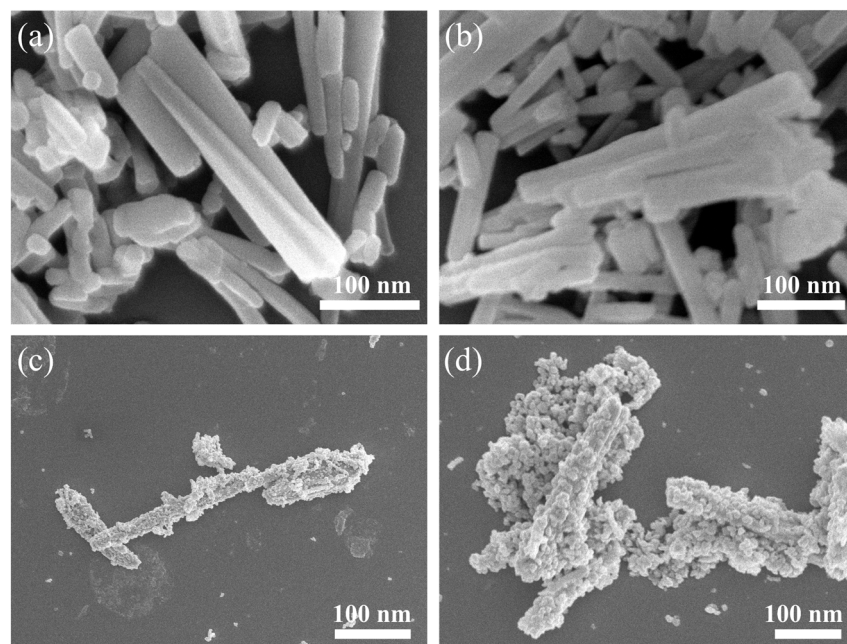


Figure 4. SEM images of (a,b) ZnO-MOF and (c,d) ZnAu-200.

TEM image of the ZnAu-200 sample is shown in Figure 5, which is basically consistent with that in SEM images. Figure 5a show high-resolution TEM (HRTEM) images of the sample. There are two distinct sets of lattice fringes in the sample, with a spacing of 0.27 nm corresponding to ZnO (002) and 0.235 nm to Au (111) planes. The energy dispersion spectrum (EDS) is shown in Figure 5b–e, illustrating the presence and distribution of Zn, Au, and O elements. Au is uniformly distributed on the surface of the sample material in the form of nanodots.

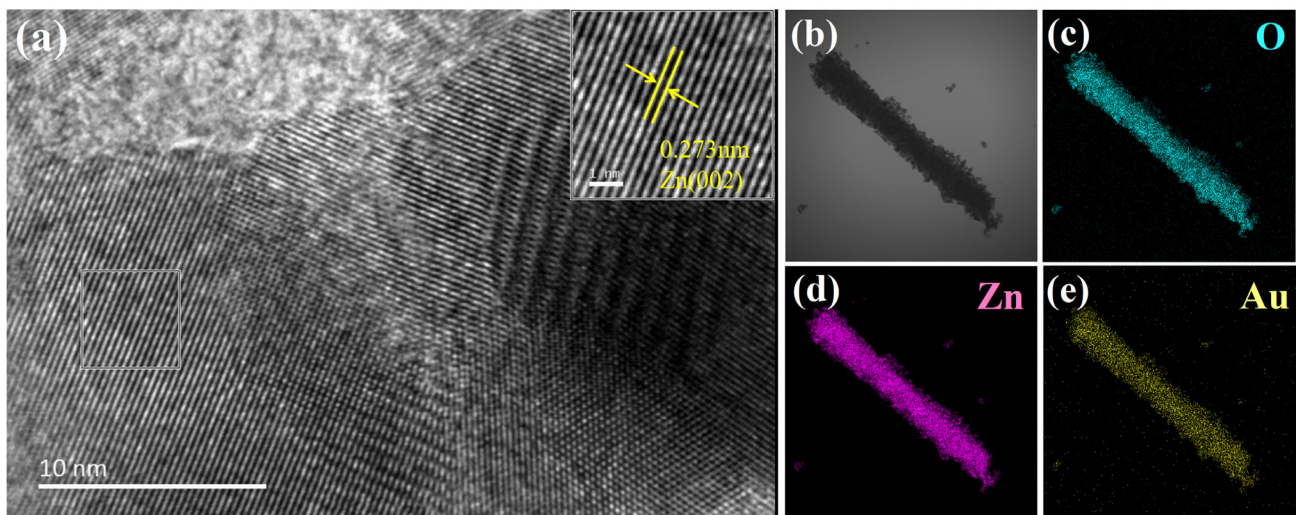


Figure 5. (a) HRTEM image and (b–e) O, Zn, and Au element mapping of ZnAu-200.

3.2. Sensing Performance

First, the optimal operating temperature of the ZnAu-200 material was determined by testing the sensor's response to 20 ppm ethyl acetate gas at different temperatures. The response of the ZnAu-200 material to the target gas changes in a volcanic curve with the change in temperature and reaches a peak value at 140 °C, as shown in Figure 6a. A temperature that is too high or too low is not conducive to the reaction between the ethyl acetate molecule and absorbed oxygen ions, so the change in the response value of the material with temperature conforms to the change law of the gas-sensitive semiconductor material [29]. This relatively low optimal response temperature helps to reduce the power consumption of the device. The curves show that the device response value shows a trend of augmenting and then decreasing with the increasing H₂AuCl₄ concentration in the modified ZnO material, reaching a maximum response value of 41.8 for the ZnAu-200 device. For comparison, the device prepared with pure ZnO has a response value of 2.4 to ethyl acetate at the same temperature. After moderate AuND modification, the response of the ZnO materials to ethyl acetate is increased by 17.4 times, which indicates that the AuND modification can improve the gas-sensitive properties of the ZnO materials. Additionally, in Figure 6b, we present the relationship between baseline resistance and temperature for pure ZnO and the three modified materials. It can be observed that as the concentration of AuCl₄⁺ ions in the modification process increases, the baseline resistance of the materials gradually increases at the same temperature. This is due to the formation of numerous Schottky junctions between the surface-modified Au nanodots and ZnO, which deepens the electron depletion layer in ZnO, leading to a higher baseline resistance. The concentration–response relationship of the ZnAu-200 sample, which has the highest performance for ethyl acetate gas, was also tested at the optimal temperature. The dynamic resistance change curve is shown in Figure 7a. The concentration–response curve shows that the device's response to the ethyl acetate gas in the range of 1–125 ppm can be linearly fitted. In tests of ethyl acetate gas at concentrations above 20 ppm, the response of the sensor tends to be saturated.

Selectivity is an important parameter to evaluate the performance of gas-sensing materials, so we tested the response of gas-sensing materials to 20 ppm methanol, acetone, ethyl acetate, ammonia, formaldehyde, and xylene gases at temperatures the above optimal reaction temperature (140 °C). As shown in Figure 6c, ZnO materials and ZnAu-100, ZnAu-200, and ZnAu-400 materials all show obvious selectivity for ethyl acetate, among which ZnAu-200 shows the best performance. The unique selectivity for ethyl acetate can be attributed to a synergistic effect between the release of more electrons by ethyl acetate molecules than other organic volatile gases in the surface reaction and the spillover effect of AuNDs [29].

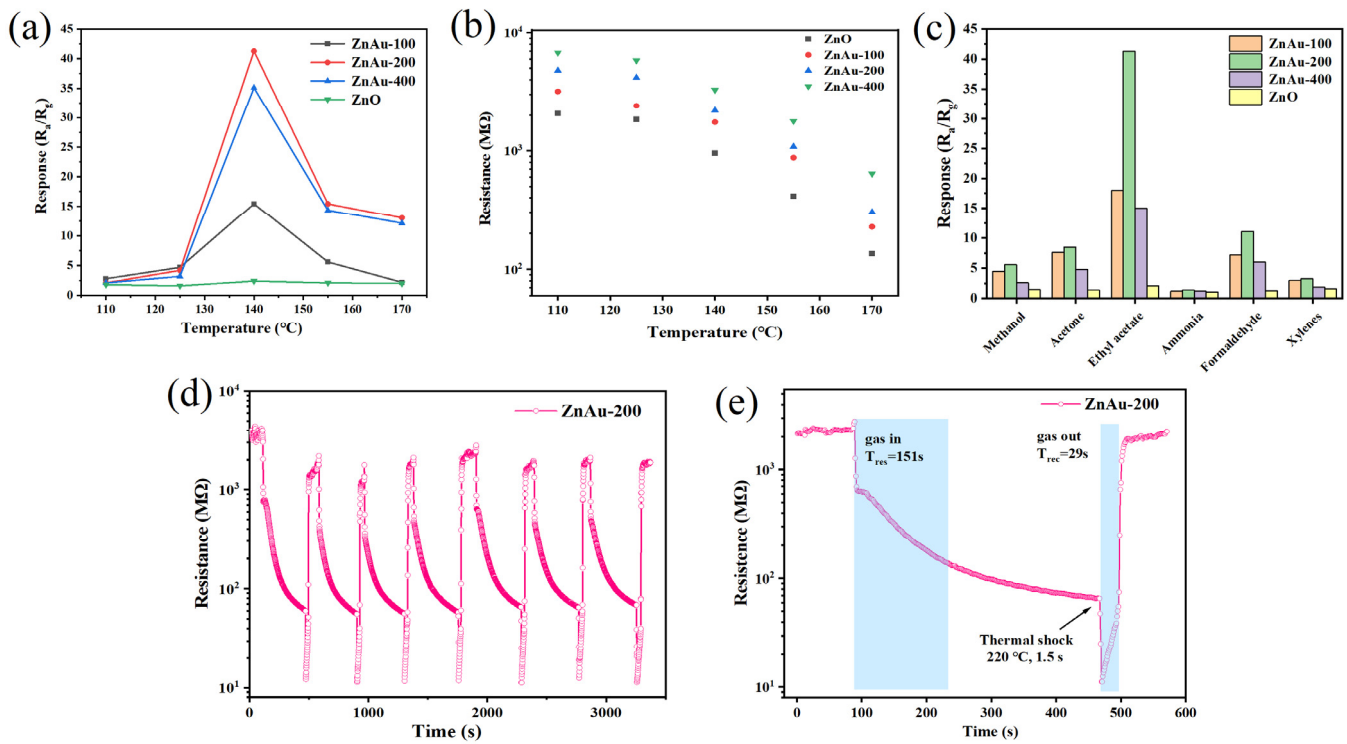


Figure 6. (a) Response–temperature relationship of sensors based on ZnAu-100, ZnAu-200, and ZnAu-400 to 20 ppm ethyl acetate; (b) the base resistance curve of the sensors at different operation temperatures; (c) responses of sensors exposed to 20 ppm of different test gases; (d) the repeatability test of ZnAu-200 sensor to 20 ppm ethyl acetate gas at 140 $^{\circ}\text{C}$ and (e) The response–recovery time curve of the ZnAu-200 sensors to 20 ppm ethyl acetate gas at 140 $^{\circ}\text{C}$.

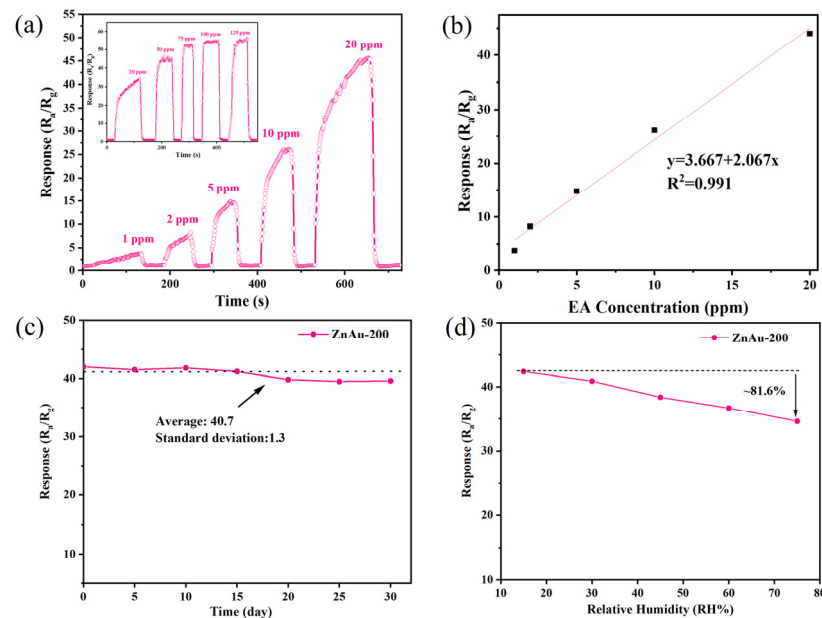


Figure 7. (a) The concentration–response curve of the ZnAu-200 sensor to 1–125 ppm ethyl acetate gas at the optimum operating temperatures; (b) the fitting line of ZnAu-200 sensor to 1–20 ppm; (c) the stability of the ZnAu-200 sensor over 30 days; (d) the response of the ZnAu-200 sensor to 20 ppm ethyl acetate under different relative humidity levels.

In practical applications, different humidity levels will affect the response value of the sensor. Therefore, we tested the response of ZnAu-200 to 20 ppm ethyl acetate under

different humidity conditions. It can be seen in the response–humidity curve in Figure 7d that the response of the sensor decreases with the increase in RH. This is caused by the fact that H₂O molecules compete with the target gas for adsorbed sites on the surface at the same time. However, the material still showed an excellent response (~81.6%) at high humidity (75% RH). In terms of stability, ZnAu-200 was tested with a 20 ppm ethyl acetate cycle, as shown in Figure 6d. In order to accelerate gas desorption during the test, a 220 °C thermal pulse was used to accelerate the recovery speed. The test results show that the material has relatively stable repeatability. At the same time, a long-term stability test on the ZnAu-200 material was conducted over 30 days, as shown in Figure 7c. The results indicate that the response of the sensor decreases with increasing time, but it still shows good long-term stability.

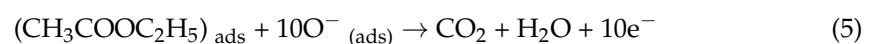
The above performance is compared with those of the reported ethyl acetate sensors, and the results are presented in Table 2. It can be seen that the sensor based on ZnAu-200 shows a higher response at a lower operating temperature, which is conducive to reducing the power consumption of the sensing device in practical applications. Moreover, the humidity stability and response values obtained under low concentrations of the sensor in this work are obviously better than those of other sensors. Therefore, sensors based on the ZnAu-200 material can be candidates for ethyl acetate detection under a variety of conditions.

Table 2. Comparison of ethyl acetate sensing results from the previous literature and this study.

Materials	OT (°C)	Conc (ppm)	Res (R _a /R _g)	LOD	Refs.
PrFeO ₃ /α-Fe ₂ O ₃ octahedrons	206	20	11	1 ppm	[29]
CoWO ₄ /α-Fe ₂ O ₃ octahedrons	206	100	24.1	1 ppm	[30]
Flower-like Au-ZnO	240	20	0.5	10 ppm	[13]
NiFe ₂ O ₄ nanoboxes	120	20	12	1 ppm	[3]
Au@ZnO nanorods	140	20	41.8	1 ppm	This work

3.3. Sensing Mechanism

As a typical N-type semiconductor material, the conductivity of ZnO is affected by the width of the depletion layer. In different gas atmospheres, the reaction of gas molecules on the surface changes the width of the depletion layer, resulting in a change in resistance. When the sensor is set in an air environment, oxygen molecules will be adsorbed on the ZnO surface and consume electrons from the surface layer, converting them into oxygen ion species. At 100–300 °C, oxygen is mainly in the form of O[−] [31]. At the same time, since the electrons inside the material are consumed by surface oxygen, a wide electron depletion layer will be formed on the surface, and the resistance will increase, as shown in Figure 6b. When the sensor is in an ethyl acetate environment, O[−] will react with the reducing gas. The reaction can be described as follows [32]:



Oxygen species react with ethyl acetate and release electrons back to the conduction band of ZnO. This reduces the electron depletion layer width of ZnO, resulting in a decrease in sensor resistance.

Compared with pure ZnO materials, ZnO modified using an in situ reduction of AuNDs exhibit higher ethyl acetate gas-sensing properties. The improvement in the performance can be attributed to the following points. First, the Au nanodots on the

nanorods help adsorb and activate more oxygen molecules and transfer them to the ZnO nanorod surface through the spillover effect [33]. This change in the proportion of oxygen molecules is reflected in the XPS test results. This chemical mechanism causes more electrons to be captured and the electron depletion layer to become wider, making the baseline resistance higher [34]. It will produce more chemisorbed oxygen and more reaction sites than original ZnO. When AuND@ZnO is exposed to ethyl acetate, more electrons will be released back to the conduction band and reduce the width of the electron depletion layer, producing a larger resistance change. Second, since the Fermi level of ZnO is higher than that of Au, electrons will be transferred from ZnO to Au nanodots at the interface between them. This forms a large number of Schottky junctions on the surface of the material, further broadening the electron depletion layer and resulting in higher baseline resistance [35–37].

The ion coordination-modified AuNDs formed on the surface of ZnO-MOF through the electrostatic adsorption of Au ions are smaller in size than those produced using common reduction methods [18,38]. When the Au particle size is small enough, a more obvious size effect will appear [39]. Such ultra-fine AuNDs will affect the ZnO lattice, thereby creating more surface defect oxygen and improving the gas-sensing properties of the material [40]. At the same time, the smaller the particle size of the gold nanodots is, the more obvious its chemical catalytic effect is, which is more conducive to the adsorption, diffusion, and reaction of the measured gas on the surface of the material [24,41]. AuNDs uniformly dispersed on the surface provide more reactive centers and exhibit higher response values. Excessive modification may cause the agglomeration of small-sized gold nanodots, weakening their catalytic effect on gas-sensing reactions [17]. This may explain the performance degradation of the ZnAu-400 sample. The above points together lead to the outstanding sensitivity of the Au@ZnO material to ethyl acetate gas.

4. Conclusions

In this study, ZnO nanorods exhibiting superior sensitivity to ethyl acetate gas were successfully prepared through in situ modification of gold nanodots on the surface of ZnO-MOF materials. Ultrafine gold nanodots uniformly distributed on ZnO nanorods play a crucial role in enhancing the gas-sensing properties. The electron spillover effect and catalysis facilitated by AuNDs on the surface of ZnO nanorods provide additional reaction centers to promote the surface reaction of ethyl acetate molecules. In situ reduction-modified ultrafine gold nanodots have an effect on the ZnO lattice, which in turn increases the adsorbed oxygen on the nanomaterial's surface. The above mechanisms collectively lead to the improvement in the gas-sensing properties of the materials. The test results demonstrate that the response of the pristine ZnO materials to 20 ppm ethyl acetate is increased by 17.4 times, reaching 41.8. Hence, AuND@ZnO nanorods can be used as a superior gas-sensitive material for ethyl acetate monitoring.

Supplementary Materials: The following supporting information can be downloaded at: <https://www.mdpi.com/article/10.3390/s24216931/s1>.

Author Contributions: All the authors contributed to the design and development of the experiments, the implementation and the writing of the paper. Specifically, conceptualization, Q.W. and W.W.; methodology, Q.W.; validation, W.W.; formal analysis, J.F. and Y.F.; investigation, Q.W. and J.F.; resources, W.W.; data curation, Q.W. and Y.F.; writing—original draft preparation, Q.W. and J.F.; writing—review and editing, Q.W., S.R. and Y.C.; supervision, S.R.; project administration, Y.C.; funding acquisition, S.R. and Y.C. All authors have read and agreed to the published version of the manuscript.

Funding: This research was funded by National Natural Science Foundation of China (Grant No. 12073009, 12374397, U21B2061).

Institutional Review Board Statement: Not applicable.

Informed Consent Statement: Not applicable.

Data Availability Statement: The authors confirm that the data supporting the findings of this study are available within the article and Supplementary Materials.

Conflicts of Interest: The authors declare no conflict of interest.

References

1. Xiang, L.J.; Wu, S.H.; Hua, Q.L.; Bao, C.Y.; Liu, H. Volatile Organic Compounds in Human Exhaled Breath to Diagnose Gastrointestinal Cancer: A Meta-Analysis. *Front. Oncol.* **2021**, *11*, 606915. [[CrossRef](#)] [[PubMed](#)]
2. Konvalina, G.; Haick, H. Sensors for Breath Testing: From Nanomaterials to Comprehensive Disease Detection. *Acc. Chem. Res.* **2014**, *47*, 66–76. [[CrossRef](#)] [[PubMed](#)]
3. Liu, N.N.; Wang, X.F.; Zhang, G.Z.; Liang, H.J.; Li, T.; Zhao, Y.H.; Zhang, T.; Tan, Z.Q.; Song, X.Z. Metal-Organic Framework-Derived Porous NiFe₂O₄ Nanoboxes for Ethyl Acetate Gas Sensors. *ACS Appl. Nano Mater.* **2022**, *5*, 14320–14327. [[CrossRef](#)]
4. Khatoon, Z.; Fouad, H.; Seo, H.K.; Alothman, O.Y.; Ansari, Z.A.; Ansari, S.G. Ethyl Acetate Chemical Sensor as Lung Cancer Biomarker Detection Based on Doped Nano-SnO₂ Synthesized by Sol-Gel Process. *IEEE Sens. J.* **2020**, *20*, 12504–12511. [[CrossRef](#)]
5. Zhang, J.; Chen, J.; Zuo, J.C.; Lan, J.S.; Jiang, Z.L.; Xiao, C.; Wang, X.H.; Zuo, Y. A novel electrochemical sensor with NiSx@MoS₂ composite for efficient NO₂[−] sensing. *Food Chem.* **2025**, *462*, 140947. [[CrossRef](#)]
6. Shi, G.L.; Hu, G.P.; Gu, L.C.; Rao, Y.; Zhang, Y.X.; Ali, F. Cataluminescence sensor based on LaCO₃OH microspheres for volatile organic compounds detection and pattern recognition. *Sens. Actuators B-Chem.* **2024**, *403*, 135177. [[CrossRef](#)]
7. Shi, G.L.; Shen, X.Y.; He, Y.G.; Ren, H. Passive Wireless Detection for Ammonia Based on 2.4 GHz Square Carbon Nanotube-Loaded Chipless RFID-Inspired Tag. *IEEE Trans. Instrum. Meas.* **2023**, *72*, 9510812. [[CrossRef](#)]
8. Ling, W.; Zhu, D.; Pu, Y.; Li, H. The ppb-level formaldehyde detection with UV excitation for yolk-shell MOF-derived ZnO at room temperature. *Sens. Actuators B-Chem.* **2022**, *355*, 131294. [[CrossRef](#)]
9. Xia, W.; Zhu, J.H.; Guo, W.H.; An, L.; Xia, D.G.; Zou, R.Q. Well-defined carbon polyhedrons prepared from nano metal-organic frameworks for oxygen reduction. *J. Mater. Chem. A* **2014**, *2*, 11606–11613. [[CrossRef](#)]
10. Li, H.Y.; Zhao, S.N.; Zang, S.Q.; Li, J. Functional metal-organic frameworks as effective sensors of gases and volatile compounds. *Chem. Soc. Rev.* **2020**, *49*, 6364–6401. [[CrossRef](#)]
11. Pentyala, V.; Davydovskaya, P.; Ade, M.; Pohle, R.; Urban, G. Metal-organic frameworks for alcohol gas sensor. *Sens. Actuators B-Chem.* **2016**, *222*, 904–909. [[CrossRef](#)]
12. Zhao, Y.M.; Wang, S.; Zhai, X.; Shao, L.; Bai, X.J.; Liu, Y.L.; Wang, T.Q.; Li, Y.N.; Zhang, L.Y.; Fan, F.Q.; et al. Construction of Zn/Ni Bimetallic Organic Framework Derived ZnO/NiO Heterostructure with Superior *N*-Propanol Sensing Performance. *ACS Appl. Mater. Interfaces* **2021**, *13*, 9206–9215. [[CrossRef](#)] [[PubMed](#)]
13. Doan, T.L.H.; Kim, J.Y.; Lee, J.H.; Nguyen, L.H.T.; Nguyen, H.T.T.; Pham, A.T.T.; Le, T.B.N.; Mirzaei, A.; Phan, T.B.; Kim, S.S. Facile synthesis of metal-organic framework-derived ZnO/CuO nanocomposites for highly sensitive and selective H₂S gas sensing. *Sens. Actuators B-Chem.* **2021**, *349*, 130741. [[CrossRef](#)]
14. Li, G.N.; Li, L. Highly efficient formaldehyde elimination over meso-structured M/CeO₂ (M = Pd, Pt, Au and Ag) catalyst under ambient conditions. *RSC Adv.* **2015**, *5*, 36428–36433. [[CrossRef](#)]
15. Guo, J.; Zhang, J.; Zhu, M.; Ju, D.X.; Xu, H.Y.; Cao, B.Q. High-performance gas sensor based on ZnO nanowires functionalized by Au nanoparticles. *Sens. Actuators B-Chem.* **2014**, *199*, 339–345. [[CrossRef](#)]
16. Xue, Z.G.; Yan, M.Y.; Yu, X.; Tong, Y.J.; Zhou, H.; Zhao, Y.F.; Wang, Z.Y.; Zhang, Y.S.; Xiong, C.; Yang, J.; et al. One-Dimensional Segregated Single Au Sites on Step-Rich ZnO Ladder for Ultrasensitive NO₂ Sensors. *Chem* **2020**, *6*, 3364–3373. [[CrossRef](#)]
17. Zhou, L.P.; Dai, S.Q.; Xu, S.; She, Y.Q.; Li, Y.L.; Leveneur, S.; Qin, Y.L. Piezoelectric effect synergistically enhances the performance of Ti₃₂-oxo-cluster/BaTiO₃/CuS p-n heterojunction photocatalytic degradation of pollutants. *Appl. Catal. B-Environ. Energy* **2021**, *291*, 120019. [[CrossRef](#)]
18. Flytzani-Stephanopoulos, M. Gold Atoms Stabilized on Various Supports Catalyze the Water-Gas Shift Reaction. *Acc. Chem. Res.* **2014**, *47*, 783–792. [[CrossRef](#)]
19. Lee, J.; Jung, Y.; Sung, S.H.; Lee, G.; Kim, J.; Seong, J.; Shim, Y.S.; Jun, S.C.; Jeon, S. High-performance gas sensor array for indoor air quality monitoring: The role of Au nanoparticles on WO₃, SnO₂, and NiO-based gas sensors. *J. Mater. Chem. A* **2021**, *9*, 1159–1167. [[CrossRef](#)]
20. Du, B.S.; Yan, F.F.; Lin, X.H.; Liang, C.Y.; Guo, X.Z.; Tan, Y.L.; Zhen, H.; Zhao, C.J.; Shi, Y.J.; Kibet, E.; et al. A bottom-up sonication-assisted synthesis of Zn-BTC MOF nanosheets and the ppb-level acetone detection of their derived ZnO nanosheets. *Sens. Actuators B-Chem.* **2023**, *375*, 132854. [[CrossRef](#)]
21. Wang, J.; Fan, S.Y.; Xia, Y.; Yang, C.; Komarneni, S. Room-temperature gas sensors based on ZnO nanorod/Au hybrids: Visible-light-modulated dual selectivity to NO₂ and NH₃. *J. Hazard. Mater.* **2020**, *381*, 120919. [[CrossRef](#)] [[PubMed](#)]
22. Ravikumar, T.; Sivaperuman, K. Fabrication of bare and cobalt-doped ZnFe₂O₄ thin film as NH₃ gas sensor with enhanced response through UV-light illumination. *Mater. Today Chem.* **2024**, *38*, 102049. [[CrossRef](#)]
23. Huang, J.Y.; Liang, H.; Ye, J.X.; Jiang, D.T.; Sun, Y.L.; Li, X.J.; Geng, Y.F.; Wang, J.Q.; Qian, Z.F.; Du, Y. Ultrasensitive formaldehyde gas sensor based on Au-loaded ZnO nanorod arrays at low temperature. *Sens. Actuators B-Chem.* **2021**, *346*, 130568. [[CrossRef](#)]

24. He, W.W.; Kim, H.K.; Warner, W.G.; Melka, D.; Callahan, J.H.; Yin, J.J. Photogenerated Charge Carriers and Reactive Oxygen Species in ZnO/Au Hybrid Nanostructures with Enhanced Photocatalytic and Antibacterial Activity. *J. Am. Chem. Soc.* **2014**, *136*, 750–757. [[CrossRef](#)] [[PubMed](#)]
25. Peng, C.; Liu, Y.L. Enhanced acetone sensing characteristics by decorating Au nanoparticles on ZnO flower-like structures. *Appl. Phys. A-Mater. Sci. Process.* **2013**, *111*, 1151–1157. [[CrossRef](#)]
26. Wang, W.; Wang, Q.L.; Fan, Y.Z.; Sun, D.; Guan, H.; Chen, Y.; Ruan, S.P. MOF-derived ZnO nanocage decorated with Nd₂O₃ nanorods for high-performance triethylamine sensing. *Sens. Actuators B-Chem.* **2023**, *389*, 133877. [[CrossRef](#)]
27. Chai, C.X.; Gao, J.; Zhao, G.Q.; Li, L.L.; Tang, Y.; Wu, C.; Wan, C.D. In-situ synthesis of ultrasmall Au nanoparticles on bimetallic metal-organic framework with enhanced electrochemical activity for estrone sensing. *Anal. Chim. Acta* **2021**, *1152*, 338242. [[CrossRef](#)]
28. Yang, M.J.; Zhang, S.D.; Qu, F.D.; Gong, S.; Wang, C.H.; Qiu, L.; Yang, M.H.; Cheng, W.L. High performance acetone sensor based on ZnO nanorods modified by Au nanoparticles. *J. Alloys Compd.* **2019**, *797*, 246–252. [[CrossRef](#)]
29. Yin, Y.Y.; Zhang, N.; Han, J.; Liu, C.X.; Adimi, S.; Wen, S.P.; Li, X.; Ruan, S.P. Metal-organic framework derived core-shell PrFeO₃-functionalized α -Fe₂O₃ nano-octahedrons as high performance ethyl acetate sensors. *Sens. Actuators B-Chem.* **2019**, *297*, 126738. [[CrossRef](#)]
30. Fan, Y.Z.; Wang, W.; Zhang, J.F.; Lu, Y.; Liu, C.X.; Adimi, S.; Zhou, J.R.; Ruan, S.P.; Chen, Y. Construction of p-n heterojunctions by modifying MOF-derived α -Fe₂O₃ with partially covered cobalt tungstate for high-performance ethyl acetate detection. *Sens. Actuators B-Chem.* **2021**, *344*, 130129. [[CrossRef](#)]
31. Meng, F.L.; Shi, X.; Yuan, Z.Y.; Ji, H.Y.; Qin, W.B.; Shen, Y.B.; Xing, C.Y. Detection of four alcohol homologue gases by ZnO gas sensor in dynamic interval temperature modulation mode. *Sens. Actuators B-Chem.* **2022**, *350*, 130867. [[CrossRef](#)]
32. Kampara, R.K.; Deenadhayalan, B.; Gopalakrishnan, J.B. Tunneling Electron Transport in ZnO Nanograins Prepared by Electrospinning Method: An Ethyl Acetate Vapour Sensor by Chemiresistive Method. *J. Porous Mater.* **2022**, *29*, 729–743. [[CrossRef](#)]
33. Nakate, U.T.; Bulakhe, R.N.; Lokhande, C.D.; Kale, S.N. Au sensitized ZnO nanorods for enhanced liquefied petroleum gas sensing properties. *Appl. Surf. Sci.* **2016**, *371*, 224–230. [[CrossRef](#)]
34. Murugesan, T.; Kumar, R.R.; Ranjan, A.; Lu, M.Y.; Lin, H.N. Fabrication of large-area Au nanoparticle decorated ZnO@ZIF-8 core-shell heterostructure nanorods for ppb-level NO₂ gas sensing at room temperature. *Sens. Actuators B-Chem.* **2024**, *402*, 135106. [[CrossRef](#)]
35. Cao, P.J.; Cai, Y.Z.; Pawar, D.; Han, S.; Xu, W.Y.; Fang, M.; Liu, X.K.; Zeng, Y.X.; Liu, W.J.; Lu, Y.M.; et al. Au@ZnO/rGO nanocomposite-based ultra-low detection limit highly sensitive and selective NO₂ gas sensor. *J. Mater. Chem. C* **2022**, *10*, 4295–4305. [[CrossRef](#)]
36. Sun, M.Q.; Wang, M.Y.; Ge, C.X.; Huang, J.R.; Li, Y.F.; Yan, P.J.; Lei, S.Y.; Wang, M.S.; Bai, L.; Qiao, G.J. Au-doped ZnO@ZIF-7 core-shell nanorod arrays for highly sensitive and selective NO₂ detection. *Sens. Actuators B-Chem.* **2023**, *384*, 133632. [[CrossRef](#)]
37. Tang, J.F.; Fang, C.C.; Hsu, C.L. Enhanced organic gas sensor based on Cerium- and Au-doped ZnO nanowires via low temperature one-pot synthesis. *Appl. Surf. Sci.* **2023**, *613*, 156094. [[CrossRef](#)]
38. Wu, C.; Zhu, X.Y.; Wang, Z.; Yang, J.; Li, Y.S.; Gu, J.L. Specific Recovery and In Situ Reduction of Precious Metals from Waste To Create MOF Composites with Immobilized Nanoclusters. *Ind. Eng. Chem. Res.* **2017**, *56*, 13975–13982. [[CrossRef](#)]
39. Lee, J.S.; Katoch, A.; Kim, J.H.; Kim, S.S. Effect of Au nanoparticle size on the gas-sensing performance of p-CuO nanowires. *Sens. Actuators B-Chem.* **2016**, *222*, 307–314. [[CrossRef](#)]
40. Do, V.H.; Prabhu, P.; Jose, V.; Yoshida, T.; Zhou, Y.T.; Miwa, H.; Kaneko, T.; Uruga, T.; Iwasawa, Y.; Lee, J.M. Pd-PdO Nanodomains on Amorphous Ru Metallene Oxide for High-Performance Multifunctional Electrocatalysis. *Adv. Mater.* **2023**, *35*, 2208860. [[CrossRef](#)]
41. Chen, Y.Z.; Wang, Z.H.; Fu, H.F.; Han, D.M.; Gu, F.B. Insights into the effect of Au particle size on triethylamine sensing properties based on a Au-ZnO nanoflower sensor. *J. Mater. Chem. C* **2022**, *10*, 3318–3328. [[CrossRef](#)]

Disclaimer/Publisher’s Note: The statements, opinions and data contained in all publications are solely those of the individual author(s) and contributor(s) and not of MDPI and/or the editor(s). MDPI and/or the editor(s) disclaim responsibility for any injury to people or property resulting from any ideas, methods, instructions or products referred to in the content.